DEVELOPMENT OF A STANDARD MARITIME C_n^2 PROFILE USING SATELLITE MEASUREMENTS

THESIS

MARCH 2015

Gregory M. Anderson, Second Lieutenant, USAF

AFIT-ENP-MS-15-M-141

DEPARTMENT OF THE AIR FORCE
AIR UNIVERSITY

AIR FORCE INSTITUTE OF TECHNOLOGY

Wright-Patterson Air Force Base, Ohio

AFIT-ENP-MS-15-M-141

DEVELOPMENT OF A STANDARD MARITIME C_N^2 PROFILE USING SATELLITE MEASUREMENTS

THESIS

Presented to the Faculty

Department of Engineering Physics and Department of Operational Sciences

Graduate School of Engineering and Management

Air Force Institute of Technology

Air University

Air Education and Training Command

in Partial Fulfillment of the Requirements for the

Degree of Master of Science (Operations Research)

Gregory M. Anderson, B.S.

Second Lieutenant, USAF

March 2015

AFIT-ENP-MS-15-M-141

DEVELOPMENT OF A STANDARD MARITIME C_N^2 PROFILE USING SATELLITE MEASUREMENTS

THESIS

Gregory M. Anderson, B.S.
Second Lieutenant, USAF

Committee Membership:

Dr. Steven T. Fiorino
Chair

Lt Col Kevin S. Bartlett, Ph.D.
Member

Dr. Kenneth W. Bauer
Member

AFIT-ENP-MS-15-M-141

Abstract

The Hufnagel-Valley (H-V) 5/7 model was developed to characterize optical turbulence (C_n^2) as it varies with height over land. While the H-V 5/7 model is not meant to predict precise values, observations will likely be in a range close to the models prediction. H-V 5/7 is not suitable for modeling turbulence over the ocean, and to date no ocean profiles have been developed. The primary objective of this research is to develop a H-V-like standard maritime model of optical turbulence, and test its ability to accurately characterize C_n^2 over a broad spatial and temporal range. Maritime temperature climatology data are obtained from the Atmospheric Infrared Sounder (AIRS) aboard NASA's Aqua satellite. Three standard models are proposed as alternatives to the H-V model. Results show that maritime profiles generally do not exhibit the surface spike in turbulence seen in H-V 5/7. Additionally, a strong latitudinal variation in the height of the C_n^2 inflection associated with the tropopause is observed, motivating the need for separate models for polar and tropic regions.

Key words: Optical turbulence, Hufnagel-Valley, Standard turbulence profile, Model fitting

Acknowledgements

I would like to thank the following people for their contributions: Dr. Steven Fiorino for his assistance and guidance as my advisor. Dr. Kevin Bartlett for his guidance as a reader, and also for introducing me to the research topic. Dr. Kenneth Bauer for his direction and guidance as a reader. David Meier for his assistance with MATLAB code and providing the starting steps for data collection. Kegan Buchhop for his excellent MATLAB coding which greatly expedited the data collection process. Dr. Brian Stone, Dr. Brian Lunday, and Dr. Jonah Reeger for answering my numerous questions and providing suggestions. Joe Han, Rebekah McKenna, Aaron Burns, and Chance Johnstone for reading over my work and providing suggestions. Chris Hergenreter for his late-night motivation, and for sharing guard-duty shifts of the COA.

Lastly, I would like to thank my body for withstanding the mental and physical conditions it was subject to in order to complete this work.

Gregory M. Anderson

Table of Contents

Page

List of Figures

List of Tables

DEVELOPMENT OF A STANDARD MARITIME C_N^2 PROFILE USING SATELLITE MEASUREMENTS

I. Introduction

1.1 Background

Optical turbulence, often quantified as the index of refraction structure constant C_n^2, affects the propagation of light [1]. It can be observed on hot days as heat on pavement radiates to create distortion, or above a fire as the rising heat causes a similar effect. Because it is the result of changing air density, optical turbulence varies widely based on atmosperic temperature conditions. Numerous optical turbulence models have been created to capture its behavior. Of interest will be standard models, which are based on thermosonde observations and aim to create a smoothed, general profile of C_n^2 as it varies with height. These models provide approximations of turbulence, but do not account for effects such as terrain or time of year. Because they are meant to be robust, they require few inputs. The most commonly used standard model is the Hufnagel-Valley (H-V) model, which has two input parameters. This model was derived using observations over White Sands Missile Range in New Mexico [2].

1.2 Problem Statement

The H-V model was developed to characterize optical turbulence as it varies with height over land. While the exact value predicted by the model may never be observed, the observed value will likely be within a range close to the model's prediction. The H-V model is effective at capturing a general trend over land, however no such model

has been created for use over the ocean. The primary objective of this research is to develop a H-V-like standard maritime model of optical turbulence, and test its ability to characterize C_n^2 trends over a broad spatial and temporal range. Additionally, the effects of location, season, and time of day are quantified.

1.3 Motivation

The High Energy Laser Joint Technology Office (HELJTO) has interest in characterizing maritime optical turbulence values for high energy laser (HEL) applications. Vertical temperature gradients can be significantly different over water as compared to land. For this reason, using a continental C_n^2 model for maritime applications could result in misleading simulations and performance predictions. HEL applications require fairly precise expected environmental envelopes for operation, and therefore a separate model should be considered. Similar laser and optics applications can also benefit from the findings of this research. Because over 70% of the earth is covered by water it seems a necessity to understand maritime optical turbulence if effective and practical laser applications are desired.

1.4 Methodology

Data utilized are from the Atmospheric Infrared Sounder (AIRS) aboard NASA's Aqua satellite. While the satellite has measurement limitations, it is assumed to be of sufficient accuracy for the application of this research. AIRS data is supplemented with observations from the National Operational Model Archive and Distribution System (NOMADS). Data are collected over ocean locations, and new standard models are derived. The models are based on observations over a wide spatial and temporal range, and are therefore adequate but not highly accurate at characterizing C_n^2 for a given location and time. The models' characterization capabilities are assessed in

comparison to the H-V model - in particular to the most commonly used variant, the H-V 5/7 model. An assessment is made on model performance as a function of altitude. Additionally, the effects of location, time of year, and time of day are studied.

1.5 Overview

Chapter two is a summary and review of scientific contributions significant to this research, as well as a background on the data collection tools used. Chapter three presents an in-depth discussion of the methodology implemented in this research. Chapter four is a discussion and analysis of significant findings and results. Chapter five provides a summary, key findings, and offers several potential directions for future work.

II. Literature Review

2.1 Optical Turbulence

Optical turbulence, denoted by the refractive index structure C_n^2, is a measure of the amount of refraction present in the air. Generally, observed values range from 10^{-12} to $10^{-16}\, m^{-2/3}$. High values (10^{-12}) indicate a turbulent atmosphere, resulting in visual blurring, such as that observed over a hot road or a fire. Low values (10^{-16}) generally indicate a negligible effect [3].

Figure 1. Jet engine causing optical turbulence [1]

Numerous models have been created to characterize C_n^2. Standard models, such as the Hufnagel-Valley model, use an equation or system of equations with few inputs to develop a generalized model. Statistical models use random number generation and Monte-Carlo simulation to capture random fluctuations present in the atmosphere. Numerical models are collections of various models, and take inputs based on the location for which a profile is desired. A discussion and comparison of the various types of models can be found in [4].

[1]Photograph used with permission from Michael Grobe (`http://grobe-bilder.com/grobe-bilder-blog/files/0120_canon_600mm_f4_l_is_usm_canon_5d_mk_ii_michael-grobe-bilder_mg_0218.jpg`).

The focus of this research is to develop a standard model similar to the H-V model.

2.2 The Hufnagel-Valley Model

The Hufnagel-Valley model was preceded by significant development of other standard profile models. A very simple model suggested by Robert Hufnagel [2] is:

$$C_n^2(h) = \begin{cases} \frac{1.5\times10^{-16}}{h} & \text{for } h \leq 20 \\ 0 & \text{for } h > 20 \end{cases} \tag{1}$$

where h is height, in meters.

This model is easy to implement, as it is only dependent on height. Hufnagel suggests that it may be a good representation of worldwide median C_n^2 values.

A slightly more complex model, known as the Hufnagel model, is:

$$C_n^2(h) = 8.2 \times 10^{-26} W^2 h^{10} e^{-h} + 2.7 \times 10^{-16} e^{-h/1.5} \tag{2}$$

with h in meters. This model has one variable input parameter, W, the root mean squared wind speed over the 5 to 20 km range; this value is typically set to 27 m/s. The Hufnagel model is only valid above the first strong inversion layer - the region near the ground where heat from the surface has a significant effect on air temperature - which is estimated to be 3 km in this case [2]. A comparison between the simple model and the Hufnagel model is shown in Figure 2. Note that height, the independent variable, is plotted on the y-axis, and C_n^2 is plotted logarithmically on the x-axis. This convention is adopted throughout the paper.

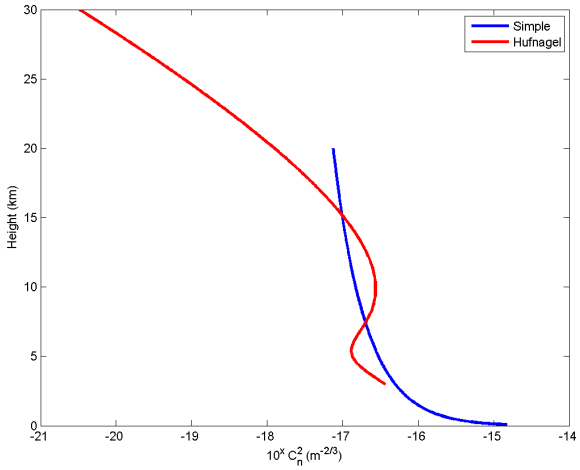

Figure 2. Simple model vs. Hufnagel model

The simple model estimates low-altitude turbulence, but is limited by a maximum height. Unlike the Hufnagel model, the simple model does not capture the bump in turbulence found at the tropopause at approximately 11 km.

Initially the Hufnagel model had a random error term, but it was removed because it was difficult to estimate or validate. The model was found to predict poorly under low tropospheric wind conditions, and for subtropical atmospheres.

The Hufnagel-Valley model was a modification of the Hufnagel model that extends C_n^2 prediction from 3 km to the ground [5]:

$$C_n^2(h) = 8.2 \times 10^{-26} W^2 h^{10} e^{-h} + 2.7 \times 10^{-16} e^{-h/1.5} + A e^{-h/0.1} \tag{3}$$

Note that this is simply the Hufnagel model with an additional term. This term was added to account for turbulence in the boundary layer. The second input, A, is the ground-level C_n^2 value. The most commonly used variant of the H-V model uses $A = 1.7 \times 10^{-14}$ and $W = 21$. This is called the H-V 5/7 model because it yields a coherence length of 5 cm and an isoplanatic angle of 7 μrad for a vertical path through the atmosphere at 0.5 μm [5]. In Figure 3, the Hufnagel model is compared

to the H-V model. Note that the Hufnagel and H-V model are identical above 3 km if the same W parameter is used.

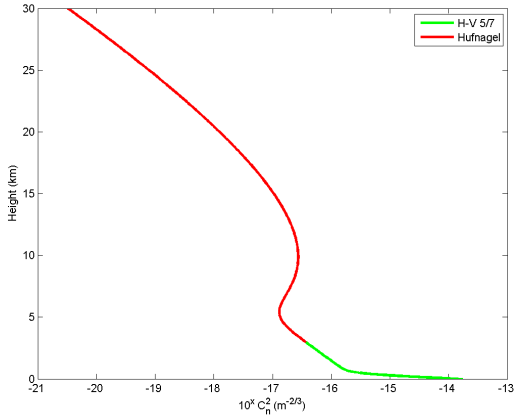

Figure 3. Hufnagel vs. H-V model.

The effect of varying the two input parameters W and A in the H-V model is demonstrated in Figures 4 and 5.

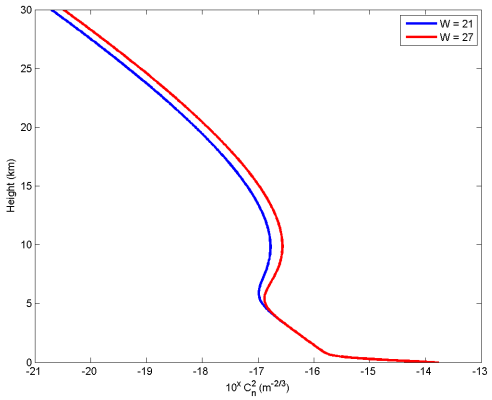

Figure 4. H-V W parameter

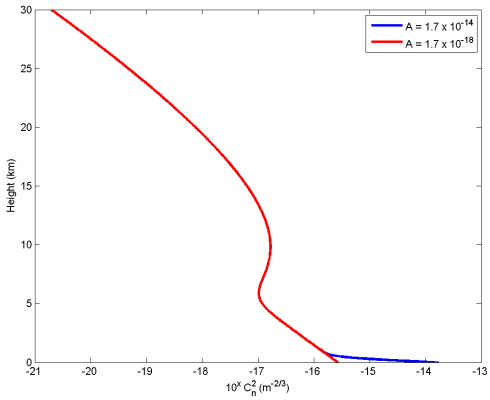

Figure 5. H-V A parameter

Changing the wind parameter shifts the model at approximately 4 km. The effect is that higher wind speed results in higher turbulence, a phenomenon that has been observed and validated. Changing the surface value parameter A results in changing

turbulence values at low altitudes. Above the first few hundred meters, there is no effect.

Distinct changes in C_n^2 behavior occur three times in the H-V model. At approximately 1 km, surface effects become negligible and turbulence decreases with height at a slower rate. The first inversion in C_n^2 occurs at approximately 5 km, and a second occurs at the tropopause (11 km).

While the H-V model is the most widely used optical turbulence profile, it still suffers from downfalls. The falloff in the boundary layer was found to be unrealistic, despite the attempt to capture turbulence in this region. Additionally, the Hufnagel model (and therefore the H-V model) was developed based on observations in White Sands Missile Range in New Mexico. It assumes a low tropopause height of 11 km. While this model may be a reasonable estimate of turbulence behavior at mid-latitude locations of similar climatology, it is not robust to the variation induced by different locations [5].

2.3 Validity of Hufnagel-Valley Model

Research has been conducted to asses the validity of the H-V standard model [4]. Gravley et al [4] compared the H-V model and other standard models to the High-Energy Laser End-to-End Operational Simulation (HELEEOS), a climatological model which contains a database of temperature, pressure, and other observations taken worldwide over a wide time range.

Agreement between H-V and HELEEOS was found to be good within the boundary layer. In the free atmosphere H-V C_n^2 follows a smooth curve with altitude, failing to account for the true fluctuations (Figure 6). The strength of the H-V model is that it is a rough best-fit line to the true observations, demonstrated by its passing through the approximate center of the HELEEOS observed values.

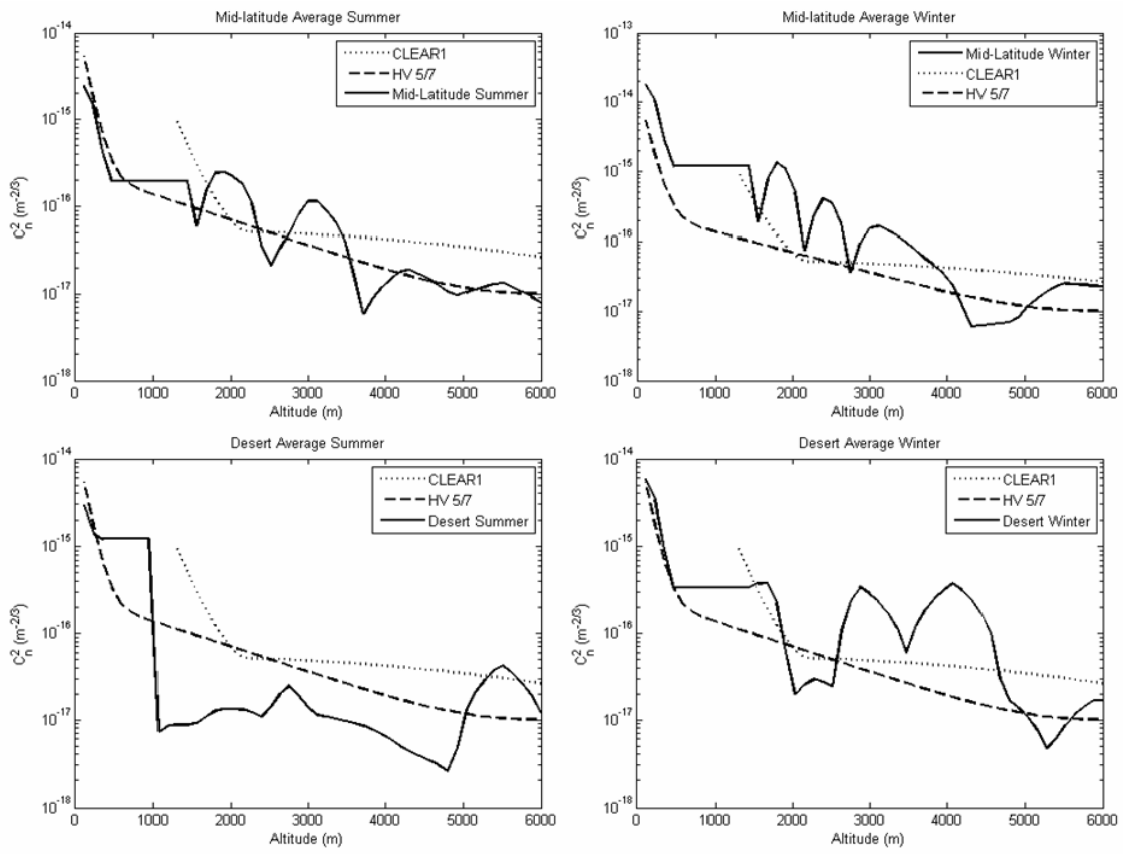

Figure 6. Comparing H-V and HELEEOS C_n^2. From Gravley [4]

Comparing distributions of C_n^2 values from H-V with HELEEOS climatological data, HELEEOS produces a distribution skewed towards smaller C_n^2 values, while H-V 5/7 results in an approximately uniform distribution (Figure 7).

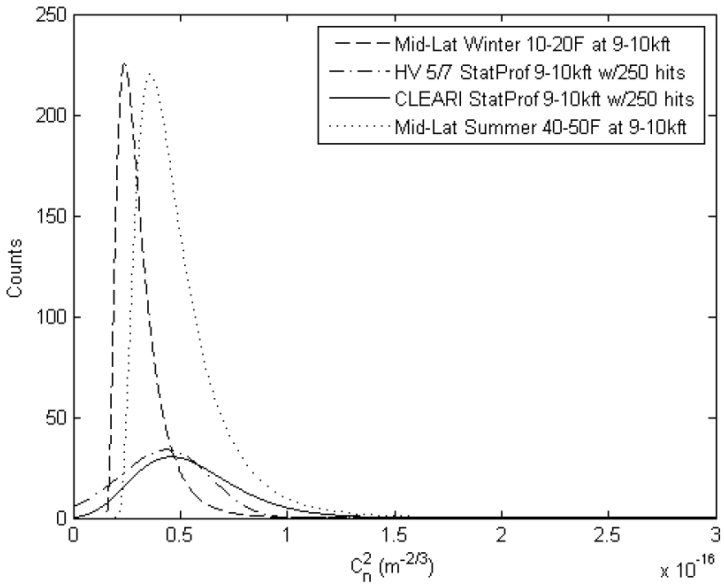

Figure 7. Distribution of H-V and HELEEOS C_n^2. From Gravley [4]

The standard model developed in this research should have similar characteristics to those seen by the H-V model.

2.4 Aqua Satellite and AIRS

This research relies on data obtained from the Atmospheric Infrared Sounder (AIRS) for modeling and analysis. AIRS is one of six instruments aboard NASA's Aqua satellite, with the primary purpose of collecting temperature and humidity profiles from the surface to 40 km. AIRS is a high-spectral-resolution sounder with 2,378 channels to measure infrared radiation (wavelengths 3.7 to 15.4 μm), and four channels measuring visible radiation (wavelength 0.4 to 0.94 μm). Its infrared channels' spatial resolution at the lowest point of observation is 13.5 km [6].

The Aqua satellite was launched in 2002 as a major contribution to the international Earth Observing System mission. It is a polar-orbiting satellite, and orbits the earth approximately every 100 minutes, crossing the equator each time. It passes over

a given location approximately twice per day, at roughly 0130 and 1330 local time. Because longitude lines converge near the poles, passes become more frequent when moving further from the equator. For areas closer to the equator where passes are less frequent, data may not be collected, based on the swath width of the measuring instrument. AIRS has too narrow of a swath width to provide day and night coverage for some areas in a single day. These missing observations are filled in on subsequent passes of the satellite [6].

2.5 Accuracy of AIRS Readings

Because archived AIRS data is available for the enitre earth and over several years, it provides an appropriate sample size for discovery of general trends. While AIRS measurement accuracy is generally high, it should not be considered an absolute measure.

The accuracy of AIRS readings for airdrop applications was studied by Meier [7]. Meier found that AIRS temperatures generally agreed closely with radiosonde measurements, with average deviations of 1 to 2 K. The study also accounted for terrain features by pairing measurements to US Geological Survey elevation data. This method proved to be successful at predicting wind speed and direction at higher altitudes - those common for airdrops - but was ineffective in the boundary layer.

In their study of AIRS measurement biases, Fetzer et al [8] attempted to measure the level of disparity in AIRS readings. When compared to the Advanced Microwave Sounding Radiometer (AMSR) aboard the same satellite as AIRS, yields were lower for AIRS than AMSR when cloud cover was high. The difference between AIRS and AMSR readings to their true value (called the observational bias) was less than 5% in most regions, but was as high as 25% in cold air outbreak regions. Additionally, when bias was at least 10%, yield was typically only 10 to 20%. Comparing AIRS to

AMSR readings, the difference (total bias) was highest when cloud cover was high. Because the radiosonde readings against which AIRS was compared are imperfect, some AIRS bias can be attributed to this random error. However, it was found to account for only 5 to 10% of AIRS's bias.

Susskind et al [9] studied the effect of cloud cover on AIRS readings. Temperature readings in the mid-troposphere were more affected by clouds than those in the stratosphere. The difference between retrieved and forecasted temperature was characterized by a slow, steady degradation as cloud cover increased, with large errors resulting only after 80% cover.

Because AIRS data are primarily collected over the ocean where cloud cover is significant, it is necessary to recognize the potential for poor AIRS yield that results in inaccurate measurements. The accuracy of AIRS is assumed to be sufficient for this research; nonetheless it is important to understand its limitations.

2.6 Supplementary Data from NOMADS

In addition to AIRS data, observations from the National Operational Model Archive and Distribution System (NOMADS) are utilized. NOMADS is a system that compiles and archives weather data collected from radiosondes, satellites, radar, and climatology models. In 2006, approximately 5 terabytes of data were accessed across over 1 million downloads each month. [10].

In particular, NOMADS winds are used because they are thought to be more accurate than those derived by AIRS.

2.7 Tatarskii's Equation

Optical tubulence values can be calculated based on an equation developed by V. Tatarskii [11] as shown in Equation 4.

$$C_n^2 = 2.8\frac{K_H}{K_M}\left(79\times10^{-6}\frac{P}{T^2}\right)L_O^{4/3}\left(\frac{\delta T}{\delta z}+\gamma_d\right)^2 \tag{4}$$

where L_O is the outer scale length of turbulence, the upper bound in size of turbulent structures; K_H and K_M are the eddy diffusivity (rate of diffusion) for heat and momentum, respectively. The ratio of eddy diffusivities is shown in Equation 5.

$$\frac{K_H}{K_M} = \begin{cases} 1/7R_i & \text{for } R_i \geq 1 \\ 6.873R_i + \frac{1}{1+6.873R_i} & \text{for } 0.01 < R_i \leq 1 \end{cases} \tag{5}$$

where R_i is the Richardson number, the ratio of potential to kinetic energy which indicates the dynamic stability of the atmosphere, as shown in Equation 6.

$$R_i = \frac{\left(\frac{g}{\bar{T}_v}\frac{\delta\bar{\theta}_v}{\delta z}\right)}{(\delta\bar{u}/\delta z)^2+(\delta\bar{v}/\delta z)^2} \tag{6}$$

In the numerator, T_v is virtual temperature, and θ_v is potential temperature. These values are used to calculate potential energy. The denominator is a measure of kinetic energy, calculated through horizontal and vertical wind gradients. These gradients are found by Equations 7 and 8.

$$\frac{\delta u_g}{\delta z} = -\frac{g}{fT}\left[\left(\frac{\delta T}{\delta y}\right)_z + \frac{\delta T}{\delta z}\left(\frac{\delta z}{\delta y}\right)_p\right] \tag{7}$$

$$\frac{\delta v_g}{\delta z} = \frac{g}{fT}\left[\left(\frac{\delta T}{\delta x}\right)_z + \frac{\delta T}{\delta z}\left(\frac{\delta z}{\delta x}\right)_p\right] \tag{8}$$

where g is the gravitational acceleration, and f is the Coriolis frequency which accounts for the rotation of the earth.

Ultimately, C_n^2 can be calculated if observed heights and their respective temperatures are known. AIRS and NOMADS data are used to calculate C_n^2 using this

method. This calculation is completely independent of the H-V model, allowing for a valid comparison between C_n^2 values derived through Tatarskii's equation and H-V profile values.

III. Methodology

3.1 Overview

The overall structure of the research is presented as a flowchart in Figure 8. AIRS and NOMADS data are collected from numerous ocean locations. The data are then analyzed to determine the behavior of tropopause height and turbulence. Because optical turblence is sporadic and noisy, the data are compiled into monthly day and night blocks for each location to allow easier characterization of the median C_n^2 value and its variation. The median values are used as observations to compare to the H-V 5/7 model, and to build new models. The predictive capability of each model is then assessed. Analysis of tropopause behavior and its accompanying C_n^2 values is used to guide model-building and parameter selection.

Software used for analysis are primarily MATLAB and JMP, a statistical analysis program.

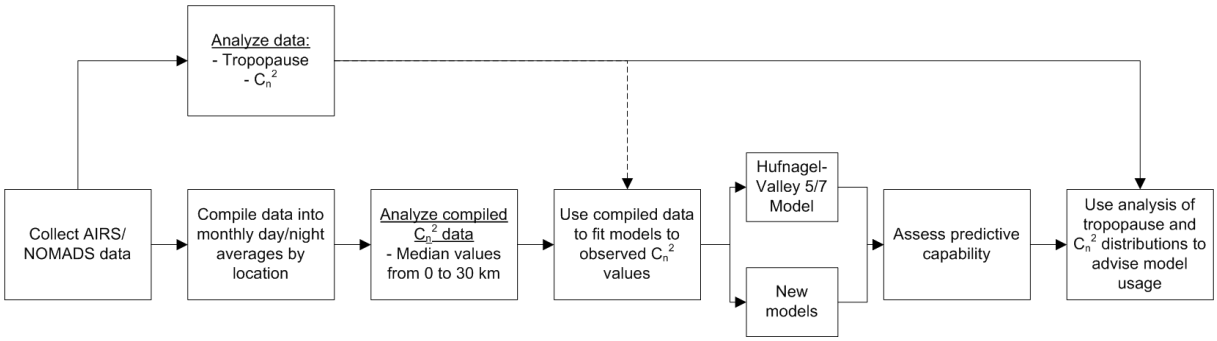

Figure 8. Methodology flowchart

3.2 Data Collection

Because the goal is to capture the general C_n^2 trend across a wide spatial and temporal range, it is necessary to collect an extensive amount of data that spans this range.

A total of 40 locations are selected and for each location, day and night observations for the entire year of 2013 are collected. This allows for day-night, seasonal, and locational comparisons to be made. The selected locations are shown in Figure 9.

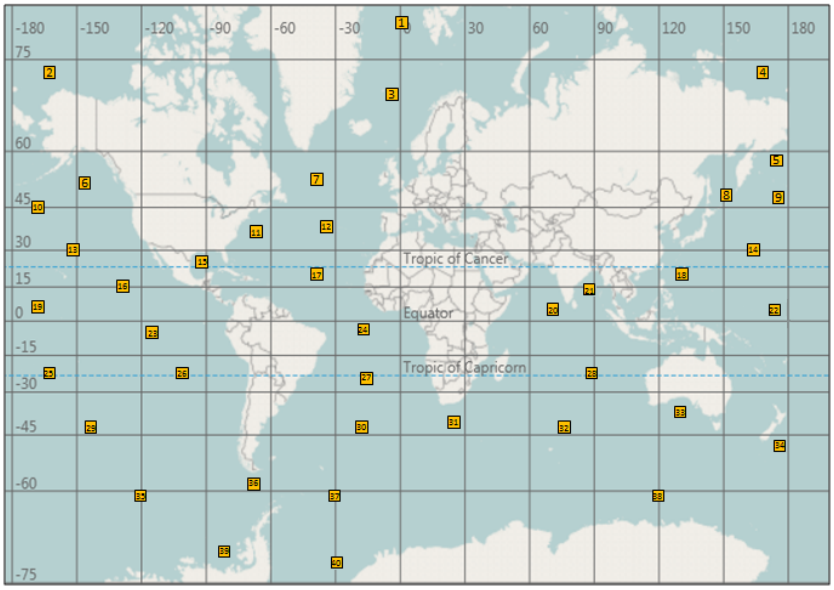

Figure 9. Collection locations

Choice of locations is such that the spread is approximately representative of the entire ocean surface. Observation locations are more dense at non-polar latitudes because characterization in this region is more important for HEL applications.

Using MATLAB code written by AFIT ENP Summer 2014 intern Kegan Bucchop, the user enters a search location, date range, and time, in order to download AIRS and NOMADS data. The files are then converted from their original format (.hdf file for AIRS and .prb file for NOMADS), and wind and temperature gradients and optical turbulence values are calculated using a methodology developed by Meier [7]. Buchhop's code was modified to automate collection over numerous locations so that no user input was required.

For each of the 40 locations, 365 days of both day and night data were sought,

for a total of 29,200 potential observed instances. In total, 23,008 observations were found, a yield of approximately 80%.

For each observed instance, approximately 100 AIRS and 30 NOMADS data points at various altitudes are found. AIRS values range from ground to approximately 70 to 80 km, while NOMADS values range up to approximately 30 km. Additionally, the resolution of AIRS measurements is higher than that of NOMADS. Meier's calculations interpolate NOMADS C_n^2 values for AIRS heights. While the data available from AIRS and NOMADS contains hundreds of climatological measures, only a small set of these is utilized. Primary data utilized in the research are the following:

AIRS data: Height, Temperature, Temperature gradient, Wind, Wind gradient, AIRS-derived C_n^2, NOMADS-derived C_n^2.

NOMADS data: Height, Temperature, Temperature gradient, Wind, Wind gradient, C_n^2.

3.3 Tropopause Analysis

The Hufnagel-Valley model makes the assumption that the tropopause is at approximately 11 km. The accompanying peak and inflection point in C_n^2 at this height is due to the change in temperature behavior when moving from the troposphere to stratosphere. Analysis of maritime tropopause behavior is used to guide model building.

To find the tropopause height, the relationship between temperature and height in the troposphere and stratosphere can be used. In the troposphere, temperature decreases with height, while in the stratosphere it increases with height. Therefore, finding the height at which temperature inflects provides a good approximation of

the tropopause.

For each of the 23,000 observations, temperature is plotted with height. A polynomial is fitted to the data, and its inflection point is found by taking the roots of its derivative. In order to obtain a better fit, only inflection points between 6 and 20 km are considered. This forces upper and lower bounds, however tropopause height is highly unlikely to be outside this range, so the restriction is considered valid.

MATLAB is used to create a 25th order polynomial fit. While this polynomial is tedious to interpret or use, only its roots (the tropopause height) and its plotted values are of interest. Lower order polynomials fail to capture the true tropopause inflection point, or misspecify it as a different point of inflection. An example of a typical fit is shown in Figure 10.

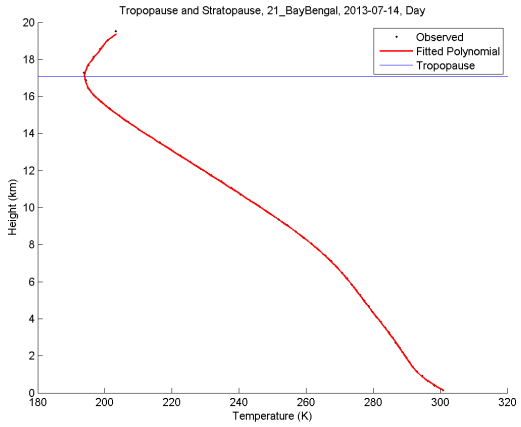

Figure 10. Polynomial fit to temperatures

A handful of 25th order fits fail to locate the tropopause due to abnormal temperature observations or lack of a prominent inflection. Most misspecified tropopause heights are above the true tropopause. To alleviate this issue, the plots are visually examined and an upper bound on tropopause is determined for each location. Tropopause heights above the bound are removed as invalid. Tropopauses above 6 km but below the true value are also removed. Examples of poor fits are shown in

Figures 11 and 12.

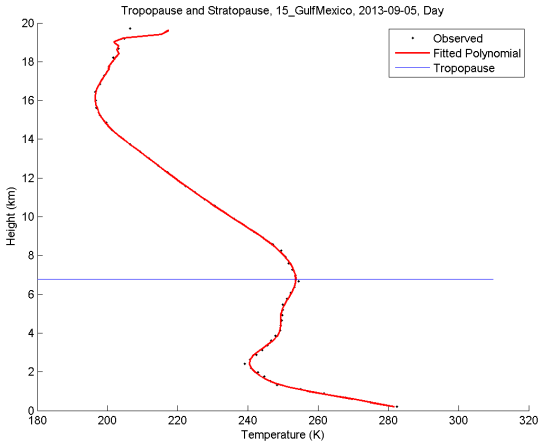

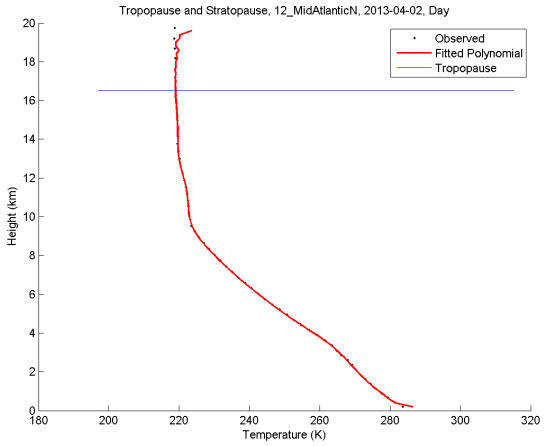

Figure 11. Wrong tropopause inflection point Figure 12. No prominent tropopause inflection

The associated wind and C_n^2 values at the tropopause are paired to each observation with the intent of discovering a relationship between some of the independent variables (location, latitude, month, time of day) and the dependent variables (tropopause, wind, C_n^2), or between dependent variables. Using JMP, the distributions of tropopause height, and tropopause C_n^2 are studied. Analysis of variance (ANOVA) and fitting of linear regression models are performed to characterize these relationships.

3.4 Data Compilation and Analysis

Because each of the 23,000 observed instances has over 100 data points associated with it, there are several million data points in total. Due to the noisy behavior of optical turbulence, it is difficult to analyze C_n^2 without cleaning up the data.

For each of the 40 locations, data are compiled by month and time of day (January Day, January Night, February Day, February Night, and so on). These combined observations are then batched into groups by height. Because NOMADS winds are used

to calculate C_n^2 and NOMADS observations are only available up to approximately 30 km, C_n^2 analysis is only performed in the range of 0 to 30 km. One hundred batches of observations (one for each 300 m) are created, and median C_n^2 is found for each batch. Rather than accounting for each observed value, this method captures the median monthly (day or night) value at various heights. Median is a more appropriate choice than mean because for a given height, C_n^2 varies by orders of magnitude and is not distributed symmetrically.

A plot of observed and median daytime C_n^2 values in April 2013 for a location north of Alaska is shown in Figure 13. The observed values represent every measured C_n^2 value during this time period.

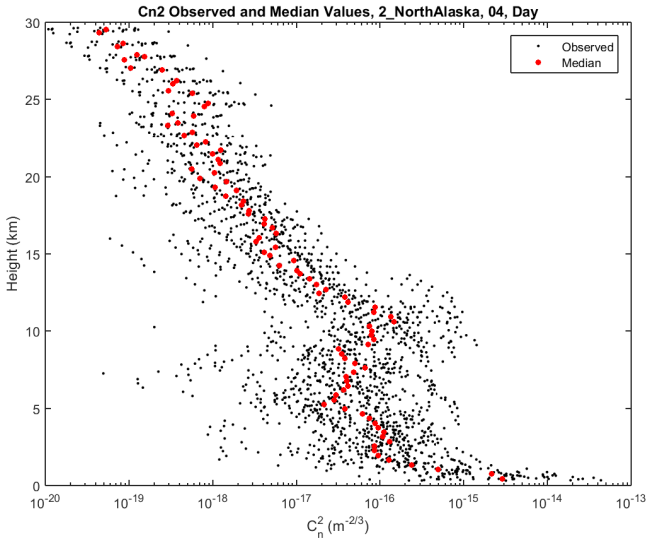

Figure 13. Observed and median C_n^2 values

While there is significant noise at some altitudes, the median values provide a good fit to the overall structure. Unless otherwise stated, "observations" will refer to calculated compiled median values for the remainder of the research. A plot of median C_n^2 is shown in Figure 14.

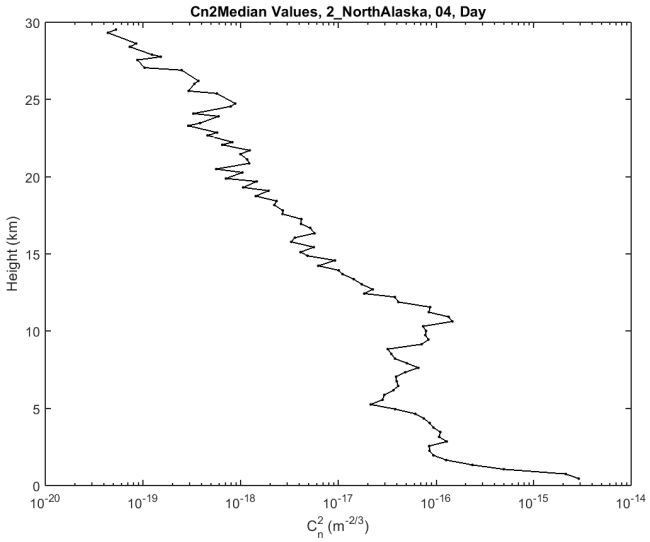

Figure 14. Median C_n^2 values.

The median plot somewhat resembles the shape of the H-V model, although its values do not match exactly. The three distinct changes in C_n^2 behavior highlighted in the H-V model in Chapter II can be observed.

3.5 Standard Models

The goal of a standard model is to capture the general C_n^2 trend with respect to altitude. This should be differentiated from a model that predicts actual C_n^2 values. Due to the complex nature of optical turbulence, a model based solely on height cannot explain enough variance to predict precise C_n^2 values.

In particular, a standard model should reasonably estimate the median C_n^2 value, and capture as many values as possible within a specified order of magnitude. Because C_n^2 varies by orders of magnitude, values are transformed with a $\log_{10}$ transformation, and assessments are performed in $\log_{10}$ space.

Several standard models are proposed and compared. The derivation and methodology used to create these models are discussed in the following sections.

Hufnagel-Valley Model.

It has been hypothesized that the Hufnagel-Valley 5/7 model is not appropriate for characterizing maritime data, largely due to its low tropopause. By fitting the H-V 5/7 model to the observed data, the hypothesis is assessed quantitatively. While any variant combination of A and W can be used to assess the H-V model, only the 5/7 variant is considered because it is most commonly used.

Polynomial Empirical Model.

A good characterization of C_n^2 can be found by fitting an empirical model to the compiled observed data. Using JMP, stepwise regression is used to fit a high-order polynomial with the best trade-off between a low number of regressor terms and low bias. Bias is primarily determined from MSE and Mallows's C_p statistic [12][1]. Because the polynomial model is a least-squares fit to the data, it achieves a near-optimal MSE. Model fitting is performed on $\log_{10} C_n^2$ values.

Dynamic Piecewise Model.

The fitted polynomial model does not have variable inputs such as W and A in the H-V model. Consequently, it is a general best-fit, but cannot be modified to reflect particular conditions. A more dynamic model is developed in piecewise fashion.

In particular, three features are accounted for: surface-level C_n^2, tropopause height, and tropopause C_n^2. The model then consists of four segments: (1) a low-altitude segment allowing for variable surface turbulence, (2) and overall best-fit to turbulence between the surface boundary layer and first inversion, (3) a dynamic fit to turbulence in the tropopause region, and (4) a best-fit to high-altitude turbulence. Figure 15 shows how these segment divisions are approximately characteristic of observed data.

[1]Mallows's C_p is a statistic that assesses the bias of a regression model. Values should not be much larger than the number of regressors.

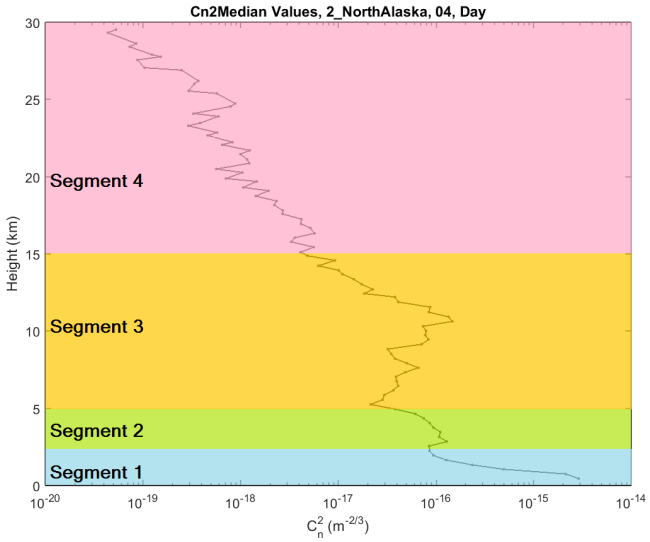

Figure 15. Example segments for the piecewise model

Segment 1 requires user-inputted surface turbulence. Surface values for particular instances can be estimated with higher accuracy than satellite measurements provide. Segments 2 and 4 are least-squares fits to the data in these regions, and are not variable. The tropopause fit in segment 3 uses piecewise cubic Hermite interpolating polynomials (PCHIP) [13] to create a differentiable function that allows tropopause height to vary based on user input. A PCHIP requires only three input points (x_1, y_1), (x_2, y_2), and (x_3, y_3). Independent monotonic cubic polynomials are then fit between (x_1, y_1) and (x_2, y_2), and between (x_2, y_2) and (x_3, y_3). MATLAB's *pchip* function is utilized, with the inputs $\mathbf{x} = [x_1, x_2, x_3]$ and $\mathbf{y} = [y_1, y_2, y_3]$.

Segment divisions are determined from inflection points observed in the polynomial empirical models.

Median Model.

A model that roughly estimates the median is created by batching observations in the same manner as that used for data compilation. The median at numerous heights

is calculated, and a polynomial fit to these medians is performed using JMP.

3.6 Model Performance

Three key metrics are used to compare models. The first metric, *mean squared error (MSE)* measures the average squared deviation of an observed value from the calculated model value. MSE can be compared between models to determine the overall quality of fit. However observations very far from the model values have more influence, which is not necessarily desired.

The second metric is the *percent of observations above (or below) the predicted model value*. An ideal model of the median has 50% of observations above its value for any height. A downside of this metric is that it only accounts for the overall spread of percentiles 0 through 50 versus percentiles 50 through 100; the variation within these ranges is not measured.

The third metric is the *percent of values within 0.5 orders of magnitude (OM) of the model value*. A range of ± 0.5 results in a prediction window of 1 order of magnitude. Unlike the first two metrics which account for the spread of observations, this one only captures observations close to the model value.

Each metric conveys different information, and while they are somewhat correlated, none can provide a full assessment alone. Together, these measures highlight the relative strengths and weaknesses of each model.

Metrics 2 and 3 are provided with respect to height and also for the model overall.

Models are assessed by their performance on the full set of observations. Additionally, the effects of location, month, and time of day are assessed through an ANOVA. Each combination of the 40 locations, 12 months, and two times of day is tested, for a total of 960 factor combinations. The proposed models are compared across the three metrics. The piecewise model's optimal surface C_n^2, tropopause height, and

tropopause C_n^2 are selected in each instance.

IV. Results

4.1 Tropopause Analysis

The distribution of tropopause heights is shown in Figure 16. The distribution is bimodal with the first peak occuring at approximately 10 km, and the second around 17 km. The variation about the first peak is significantly greater than about the second.

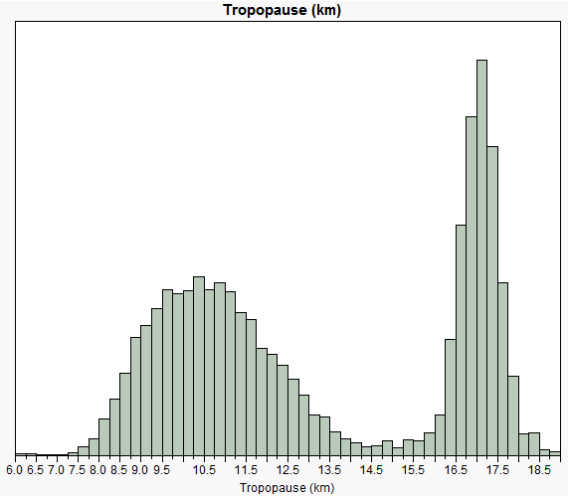

Figure 16. Distribution of tropopause heights.

While the mean tropopause height is 13.25 km, from the histogram it can be seen that this value is not representative of a likely occurence. An ANOVA on the effect of location reveals that there are two distinct groups which are divided by latitude. Locations 1 through 13 and 29 through 40, which are more polar regions, have a low tropopause. Locations 14 through 28, in the tropics, have a high tropopause. Tropic observations are located within the red band in Figure 17. Tropopause histograms by region are shown in Figure 18.

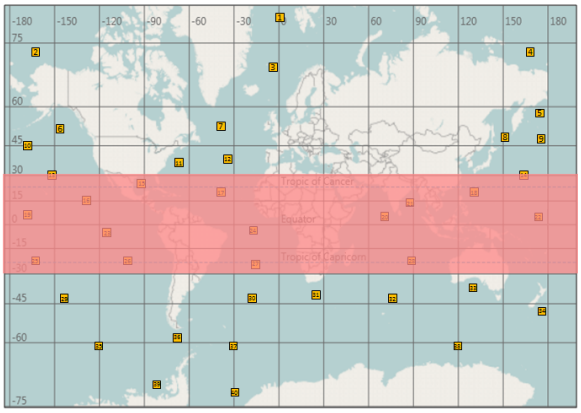

Figure 17. Polar and tropic locations

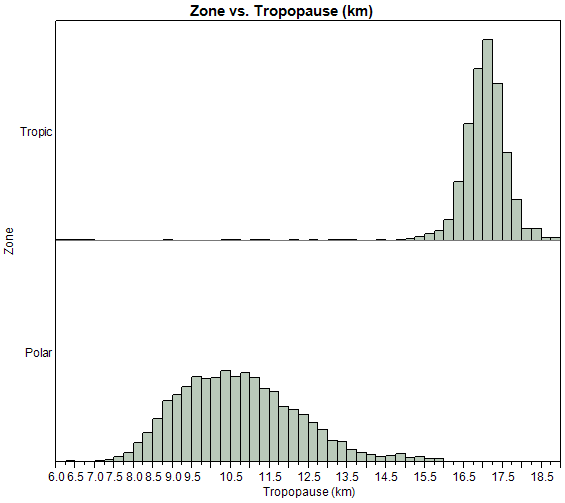

Figure 18. Tropopause height by region

17

It may be somewhat counterintuitive that there is a discrete boundary at which tropopause height drops significantly instead of a gradual, continuous change with latitude. However, the results discovered here have been validated in a study by Birner et al [14]. It was found that "the edges of the tropical belt can be located at the latitudes of an abrupt change in tropopause height, at about 34° N and 33° S."

The data are therefore divided into polar and tropic regions and analyzed individually, rather than fitting a single model to all of the observations.

4.2 Data Discontinuity

A plot of C_n^2 observations reveals a discontinuity at approximately 24.5 km, where turbulence increases suddenly (Figure 19). Approximate linear fits above and below 24.5 km are provided to highlight the shift.

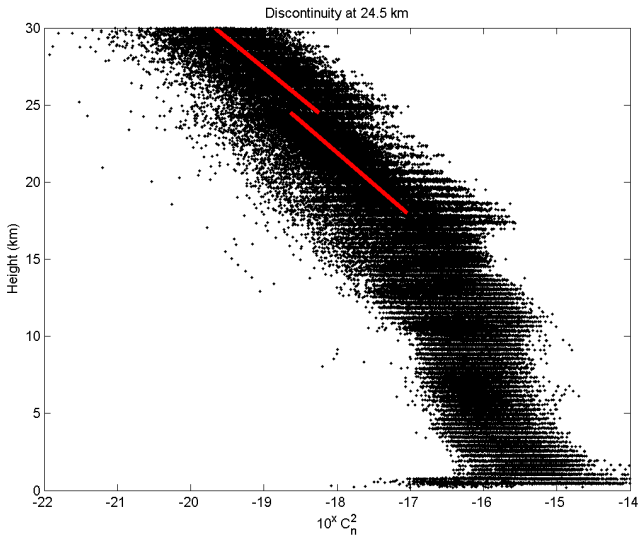

Figure 19. Discontinuity in C_n^2 values

This behavior is not characteristic of C_n^2, however it appears to occur for the majority of observations. The problem is likely due to an error in the interpolation of NOMADS C_n^2 for AIRS heights. Therefore fitted models are appropriate for the data but not necessarily effective in the 24.5 to 30 km range.

4.3 Overall Model Assessment

Hufnagel-Valley Model.

The results of fitting the H-V 5/7 model to the polar and tropic data are shown in Figures 20 and 21.

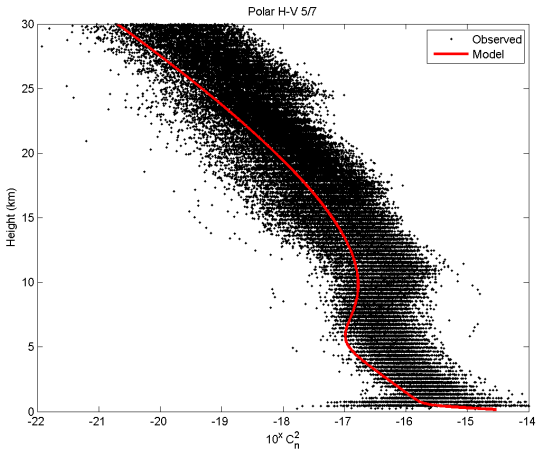

Figure 20. H-V 5/7 model in polar region

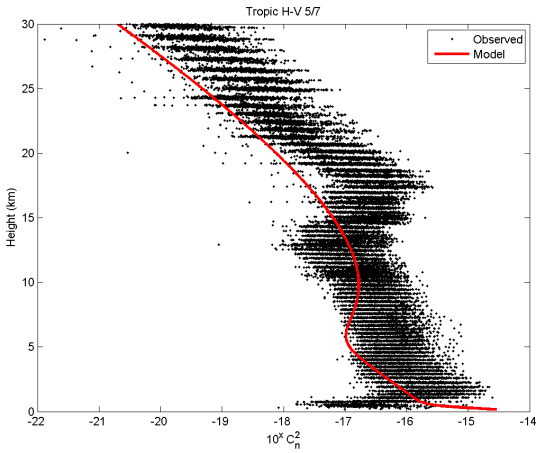

Figure 21. H-V 5/7 model in tropic region

Both models are extremely poor fits. While the 11 km tropopause height is appropriate for the polar data, it is very inaccurate for the tropic data where the tropopause is at nearly 17 km. As suggested by the plots, MSE is lower for polar data (0.438) than it is for tropic data (0.551). Still, neither fit is characteristic of the general C_n^2 trend. Metrics of H-V 5/7 model performance for polar and tropic regions are shown in Figures 22 and 23, respectively.

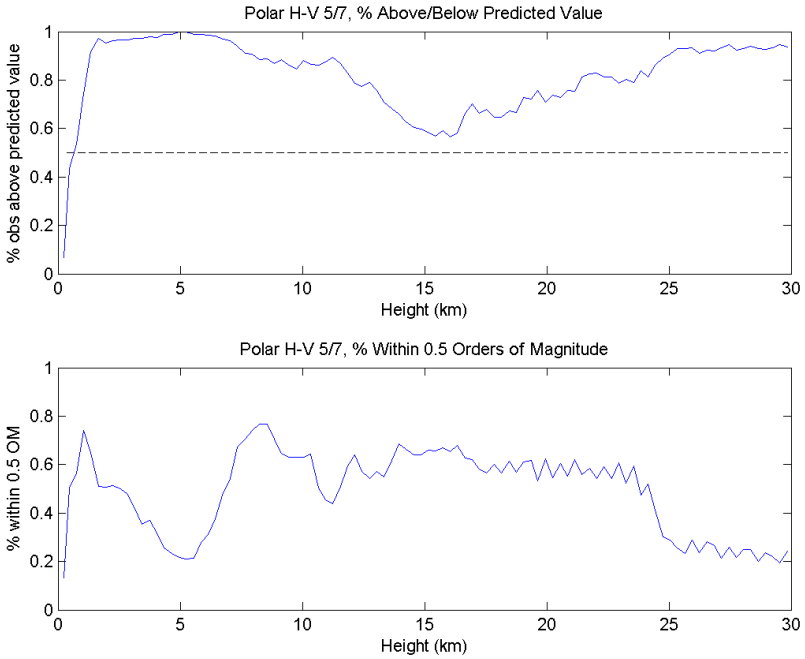

Figure 22. H-V 5/7 polar performance

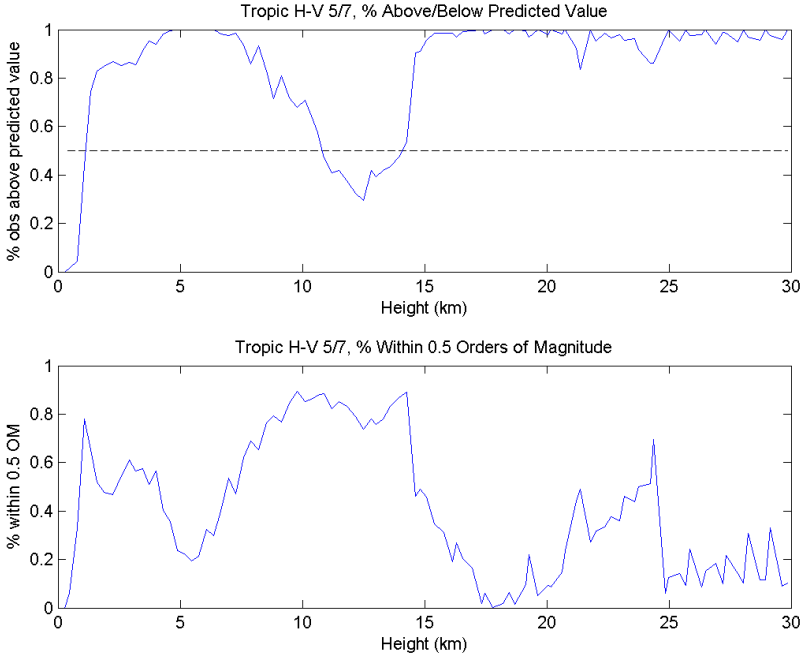

Figure 23. H-V 5/7 tropic performance

In both regions the model underestimates C_n^2 for nearly the entire 0 to 30 km range. The model's polar performance is more consistent than in the tropic region, however it never approaches a median approximation. As seen in Figure 23, in the range of approximately 8 to 13 km, the tropic model predicts 70 to 80 percent of observations within 0.5 orders of magnitude and reasonably predicts the median. Based on the overall fit of the model, this is attributed purely to chance. Performance in both regions drops significantly at around 25 km. Overall model performance is summarized in Table 1.

Table 1. H-V 5/7 Model Performance

Model	MSE	Pct Above	Pct Within 0.5 OM
Polar	0.428	0.826	0.502
Tropic	0.570	0.828	0.436

Polynomial Models.

Polynomial fits to polar and tropic observations are shown in Figures 24 and 25.

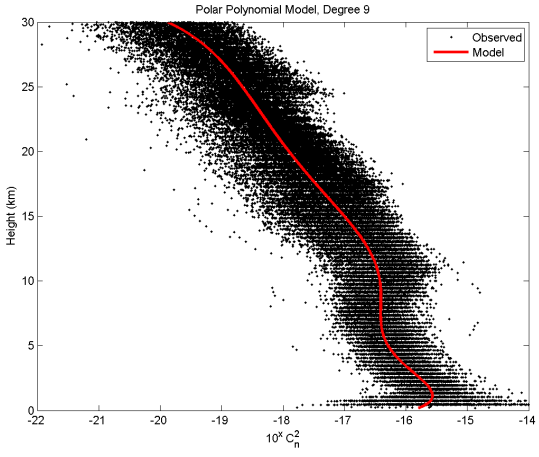

Figure 24. 9th order polar polynomial model

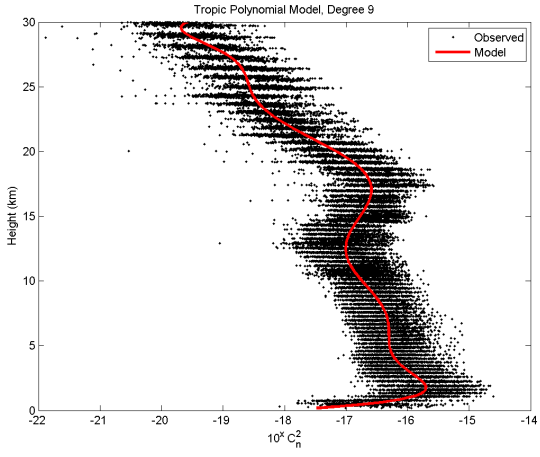

Figure 25. 9th order tropic polynomial model

The models are expressed in Equations 9 and 10.

Polar: $log_{10}(C_n^2(h)) = -15.903 + 0.685h - 0.439h^2 + 0.0987h^3 - 0.0114h^4 + 0.00076h^5$
$$-3.01 \times 10^{-5}h^6 + 7.16 \times 10^{-7}h^7 - 9.33 \times 10^{-9}h^8 + 5.11 \times 10^{-11}h^9 \quad (9)$$

Tropic: $log_{10}(C_n^2(h)) = -18.117 + 3.854h - 2.240h^2 + 0.613h^3 - 0.093h^4 + 0.0083h^5$
$$-0.00044h^6 + 1.41 \times 10^{-5}h^7 - 2.42 \times 10^{-7}h^8 + 1.74 \times 10^{-9}h^9 \quad (10)$$

where h is height, in km.

These models provide very good characterization of observed C_n^2, featuring small fluctuations not seen in the H-V model. MSE for the polar and tropic models are 0.193 and 0.139, respectively. The tropopause inflection in C_n^2 for both models occurs close to the average tropopause height for the region. The tropic model has another inflection point near 30 km, a feature in contrast with the H-V model and theoretical C_n^2 behavior. The polar model is more well-behaved than the tropic model; from 10 to 20 km the relationship between height and turbulence is approximately linear.

Model metrics are shown in Figures 26 and 27.

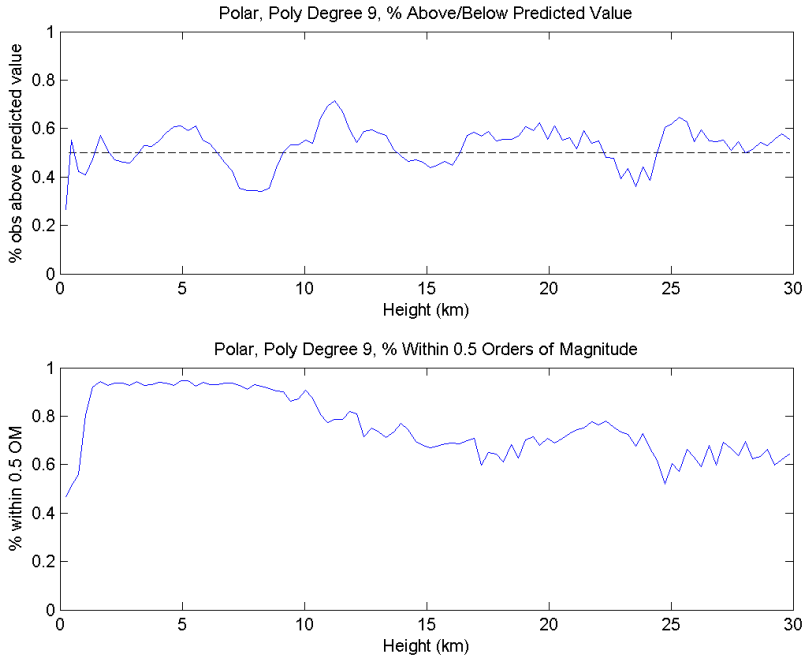

Figure 26. 9th order polar polynomial performance

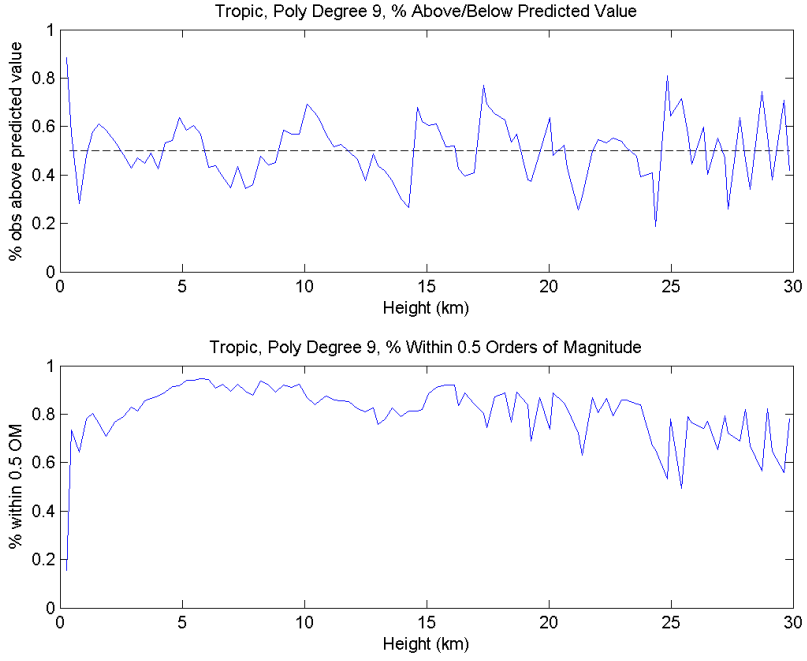

Figure 27. 9th order tropic polynomial performance

Performance has improved immensely over the H-V model. Predicted values are close to the median, with stronger deviations observed for the tropic model. At low altitudes both models predict approximately 90 percent of values within 0.5 OM. Prediction drops for the polar model above 10 km, but remains high for the tropic model. Overall performance is summarized in Table 2.

Table 2. Polynomial Model Performance

Model	MSE	Pct Above	Pct Within 0.5 OM
9th Order Polar	0.193	0.525	0.768
9th Order Tropic	0.139	0.501	0.832

The tropic model performs slightly better than the polar model, however both have low MSE, do well at characterizing the median, and provide a window that captures the majority of observed values.

Dynamic Piecewise Models.

Insights gained from the polynomial models are used to build the piecewise models. Divisions between segments 1 and 2 (occuring at height h_1) and between segments 2 and 3 (at height h_2) are found by the inflection points of the polynomial models. Turbulence above the tropopause is well behaved, so the division between segments 3 and 4 at height h_3 is approximated. Tropopause height h_t varies based on user input, however for model comparison it is set to the tropopause height found by the polynomial model. [1] The piecewise model is then derived in the following manner:

1. A third-order polynomial fit is made to segment 2. This model is used to determine $C_n^2(h_1)$ and $C_n^2(h_2)$.

[1] No root is found in the tropopause for the 9th order model, so the 10th order root is used instead.

2. A linear fit is made between user-inputted surface turbulence $C_n^2(0)$ and $C_n^2(h_1)$.

3. A third-order polynomial fit is made to segment 4. This model is used to determine $C_n^2(h_3)$.

4. PCHIP are fitted between points $(h_2, C_n^2(h_2))$, $(h_t, C_n^2(h_t))$, and $(h_3, C_n^2(h_3))$.

The critical points h_i and $C_n^2(h_i)$ used for model testing are shown in Table 3. Bold values are variable based on user input.

Table 3. Piecewise Critical Values

	Polar		Tropic	
Coord.	Height	$\log_{10} C_n^2$	Height	$\log_{10} C_n^2$
$(0, C_n^2(0))$	0	**-15.84**	0	**-17.75**
$(h_1, C_n^2(h_1))$	1.16	-15.46	1.75	-15.66
$(h_2, C_n^2(h_2))$	7.49	-16.49	12.50	-17.13
$(h_t, C_n^2(h_t))$	**9.75**	**-16.38**	**17.06**	**-16.59**
$(h_3, C_n^2(h_3))$	15	-17.04	23	-18.43

In the polar region, a relationship exists between latitude and tropopause height. However a fitted model that predicts tropopause height based on latitude yields poor goodness-of-fit[2], so its use is not advised. The relationship does not exist in the tropic region.

Plots of the models are shown in Figures 28 and 29. Critical heights are added to highlight the piecewise segments.

[2]This assessment is based on the regression lack of fit test

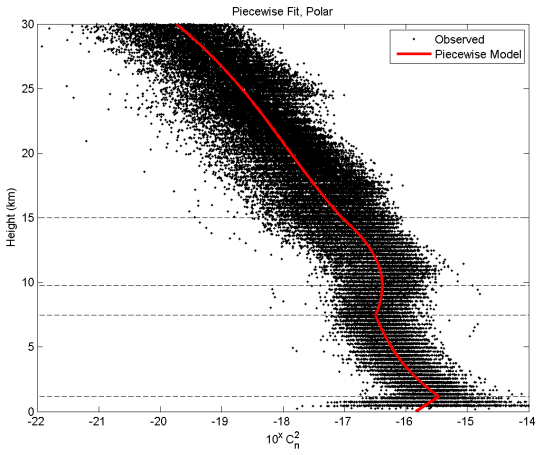

Figure 28. Piecewise polar model

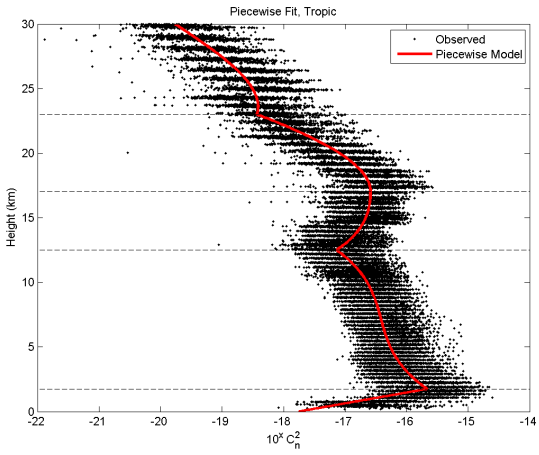

Figure 29. Piecewise tropic model

The models are specified in Equations 11 through 15.

$$log_{10}(C_n^2(h)) = \begin{cases} C_n^2(0) + \frac{C_n^2(h_1) - C_n^2(0)}{h_1} h & \text{for } 0 \leq h \leq h_1 \\ p_2 & \text{for } h_1 \leq h \leq h_2 \\ C_n^2(h_2) + x_{11}(h - h_2) + x_{12}(h - h_2)^2 + x_{13}(h - h_2)^3 & \text{for } h_2 \leq h \leq h_t \\ C_n^2(h_t) + x_{21}(h - h_t) + x_{22}(h - h_t)^2 + x_{23}(h - h_t)^3 & \text{for } h_t \leq h \leq h_3 \\ p_4 & \text{for } h_3 \leq h \leq 30 \end{cases} \tag{11}$$

For the polar region,

$$p_2 = -15.085 - 0.36h + 0.0325h^2 - 0.0013h^3 \tag{12}$$

$$p_4 = -11.55 - 0.63h + 0.023h^2 - 0.00038h^3 \tag{13}$$

For the tropic region,

$$p_2 = -14.98 - 0.484h + 0.059h^2 - 0.0028h^3 \tag{14}$$

$$p_4 = -81.2 + 6.799h - 0.238h^2 + 0.0027h^3 \tag{15}$$

Coefficients x_{11} through x_{23} are calculated using MATLAB's *pchip* function. The inputs are $\mathbf{x} = [h_2, h_t, h_3]$ and $\mathbf{y} = [C_n^2(h_2), C_n^2(h_t), C_n^2(h_3)]$. Using *variablename* = *pchip*$(\mathbf{x}, \mathbf{y})$, the value *variablename.coefs* gives a 2×4 array of the coefficients, in the form

$$\begin{bmatrix} x_{13} & x_{12} & x_{11} & C_n^2(h_2) \\ x_{23} & x_{22} & x_{21} & C_n^2(h_t) \end{bmatrix}$$

The first row is the coefficients for the range h_2 to h_t, and the second row is the coefficients for the range h_t to h_3.

Model metrics are shown in Figures 30 and 31.

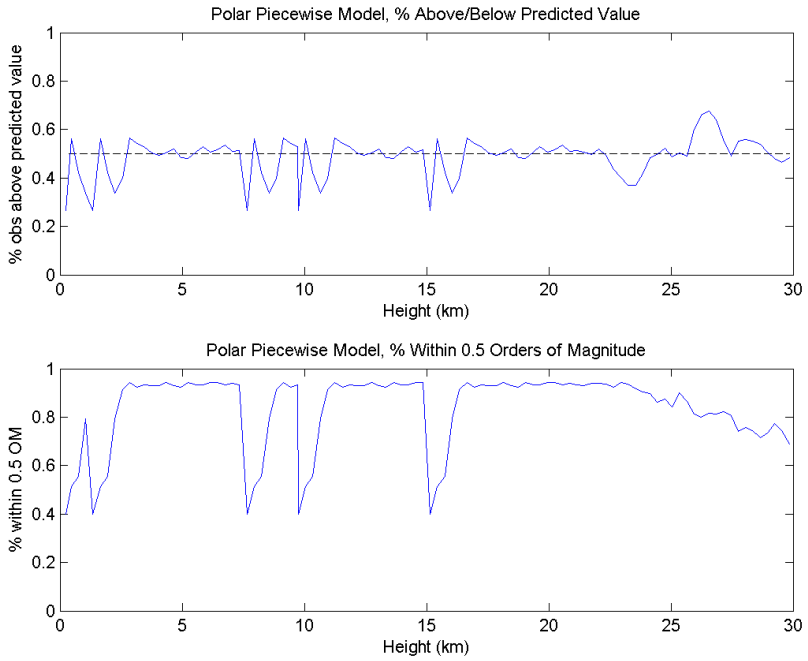

Figure 30. Polar piecewise model performance

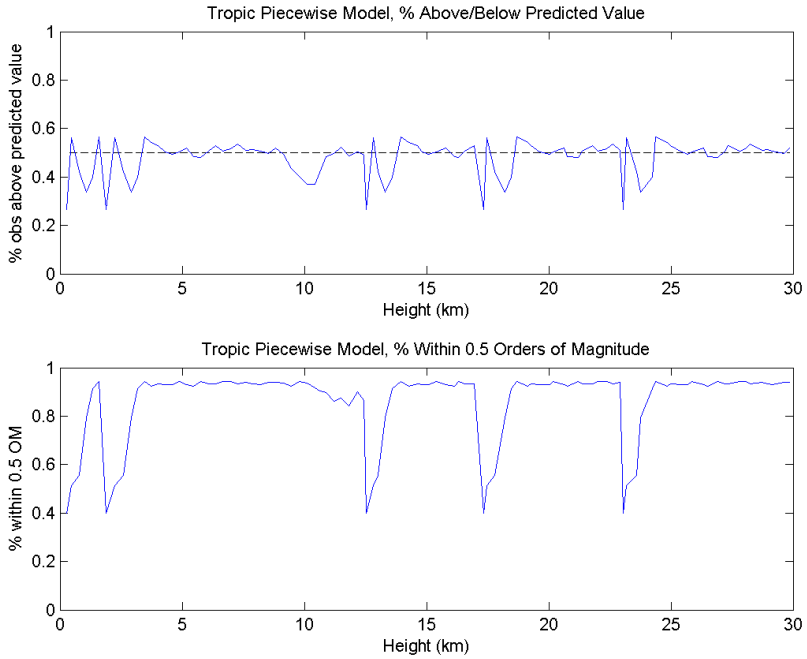

Figure 31. Tropic piecewise model performance

Significant drops in performance are observed at the critical heights for both the polar and tropic model, suggesting that enforcing continuous segments sacrifices model adequacy. Outside of these heights, the models outperform their polynomial counterparts. Summary statistics for the piecewise models are shown in Table 4.

Table 4. Piecewise Model Performance

Model	MSE	Pct Above	Pct Within 0.5 OM
Polar	0.193	0.517	0.769
Tropic	0.150	0.502	0.818

Overall performance is comparable to the polynomial models, with a slight increase in MSE for the tropic region. The true applicability of the piecewise models is not assessed by holding the variable parameters constant, therefore the test across all factor combinations will be more telling.

Median Models.

The results of fitting polynomial models to median values are shown in Figures 32 and 33.

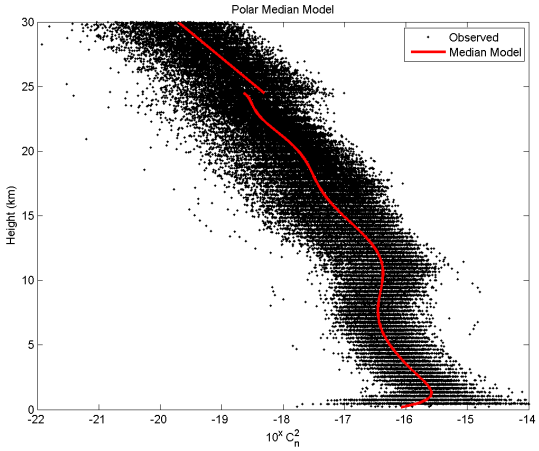

Figure 32. Polar median model

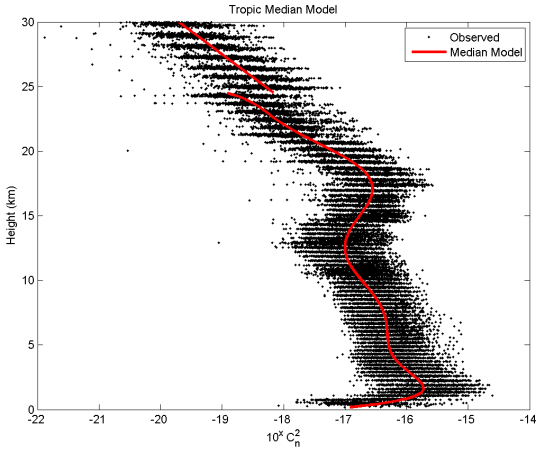

Figure 33. Tropic median model

The shift in median C_n^2 at 24.5 km is very apparent in these models, resulting in poor continuous fits. Piecewise models are constructed to alleviate this issue. The models are presented in Equations 16 through 20:

$$log_{10}(C_n^2(h)) = \begin{cases} Med_1^{Region}(h) & \text{for } 0 \leq h \leq 24.5 \text{ km} \\ Med_2^{Region}(h) & \text{for } h > 24.5 \text{ km} \end{cases} \tag{16}$$

where

$$Med_1^{Polar}(h) = -16.320 + 1.538h - 1.154h^2 + 0.411h^3 - 0.089h^4 + 0.012h^5 \\ -0.001h^6 + 6.16 \times 10^{-5}h^7 - 2.12 \times 10^{-7}h^8 + 4.05 \times 10^{-9}h^9 - 3.29 \times 10^{-10}h^{10} \tag{17}$$

$$Med_2^{Polar}(h) = -12.068 - 0.255h \tag{18}$$

$$Med_1^{Tropic}(h) = -17.366 + 2.668h - 1.545h^2 + 0.405h^3 - 0.057h^4 + 0.005h^5 \\ -0.00021h^6 + 4.91 \times 10^{-6}h^7 - 4.77 \times 10^{-8}h^8 \tag{19}$$

$$Med_2^{Tropic}(h) = -11.266 - 0.281h \tag{20}$$

Figures 34 and 35 provide metrics for the median models.

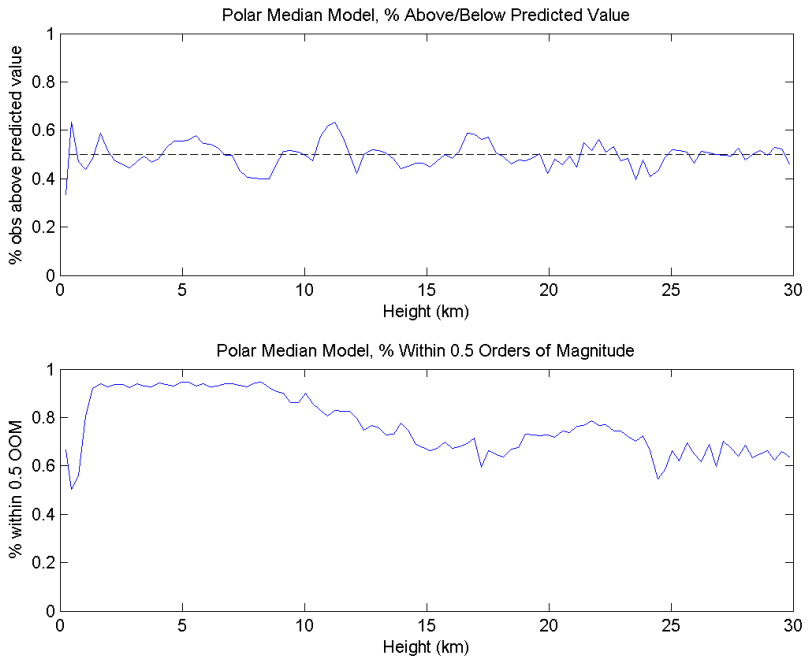

Figure 34. Polar median model performance

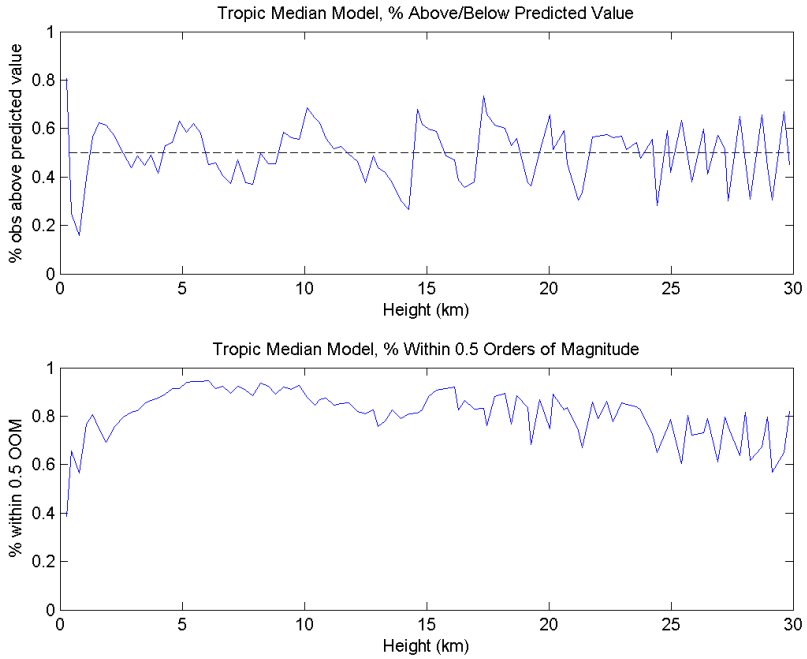

Figure 35. Tropic median model performance

As expected, both models are good characterizations of the median; observation distributions are centered around the 50% line, and a large number of observed values are within 0.5 OM. The metrics for the median models appear very similar to those of the polynomial models. The decline in prediction for the polar model is observed in both cases, as are the abrupt deviations for the tropic models. Model summary statistics are shown in Table 5.

Table 5. Median Model Performance

	Height	MSE	Pct Above	Pct Within 0.5 OM
Polar	0 to 24.5 km	0.175	0.499	0.780
	24.5 to 30 km	0.295	0.499	0.647
	Overall	**0.193**	**0.499**	**0.776**
Tropic	0 to 24.5 km	0.131	0.498	0.844
	24.5 to 30 km	0.190	0.473	0.761
	Overall	**0.138**	**0.495**	**0.834**

4.4 Model Testing

The H-V 5/7, polynomial, and piecewise models are tested on each combination of location, month, and time of day. The appropriate polynomial and piecewise model for the region is used. In each instance, the piecewise model's surface C_n^2 value is extrapolated based on the observed points at low altitude. Tropopause height and C_n^2 are the median observed values at the location being tested. The effect of the variable parameters is demonstrated in Figures 36 and 37.

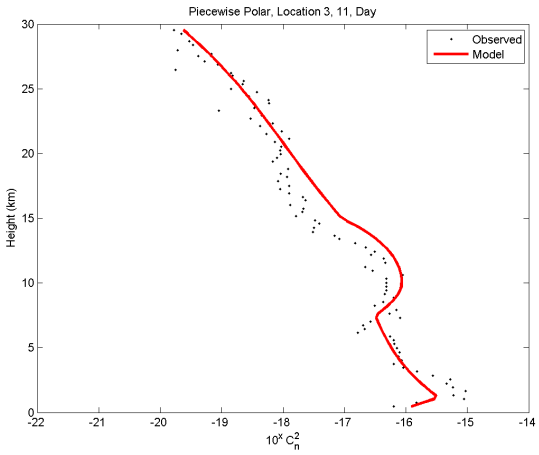

Figure 36. Piecewise model for location 17

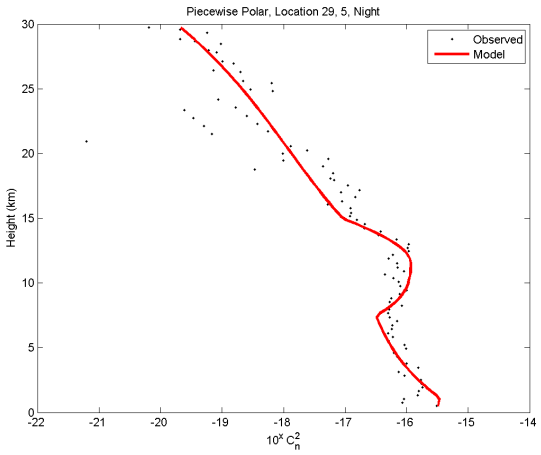

Figure 37. Piecewise model for location 28

For each metric, significant differences across models are found with p-value $<$ 0.0001. Overall, the polynomial models perform the best on all metrics at Tukey test significance 0.05. The results of the tests are summarized in Table 6.

Table 6. Model Metrics - Mean Values

Model	MSE	Pct Above	Pct 0.5 OM
H-V 5/7	0.503	0.827	0.478
Polynomial	**0.181**	**0.515**	**0.791**
Piecewise	0.238	0.437	0.773

Analysis is also performed across each of the factors. Comparing each model in both polar and tropic zones, MSE is lowest for the polynomial model in the tropics (0.145), and the polynomial models are also closest to a 50-50 spread. In the tropics, the polynomial and piecewise models both capture at least 80% of observations within 0.5 OM.

Dividing the data by season[3], several interesting trends are found. The lowest MSE is achieved by the polynomial models in all seasons, and the piecewise models in winter and spring. In the spring and winter, the piecewise models have the best overall spread of values above and below. The H-V model severely underpredicts, while the piecewise models slightly overpredict in summer and fall. In spring, the polynomial and piecewise models again have over 80% of values within 0.5 OM. Stratification by this metric across other season-model cominbations is divided completely by model, with the polynomial, piecewise, and H-V models ranking from best to worst.

For each factor combination, the winning model can be considered the one with the optimal metric value (minimum MSE, closest to 50% above/below, maximum

[3]In the northern hemisphere, December, January, and February are considered winter, March-May are spring, June-August are summer, and September-November are fall. The opposites are used in the southern hemisphere.

percent within 0.5 OM). Counts of winning models are shown in Figures 38 through 40. These charts convey the change in performance for each model across factor levels.

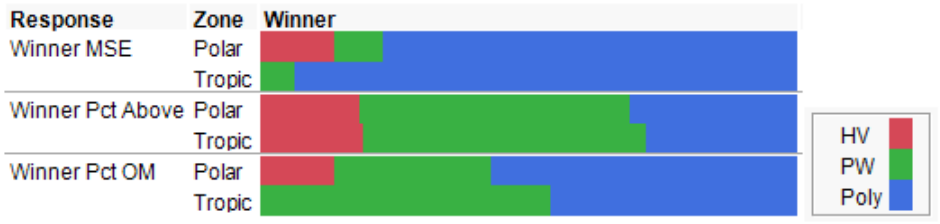

Figure 38. Model performance by zone

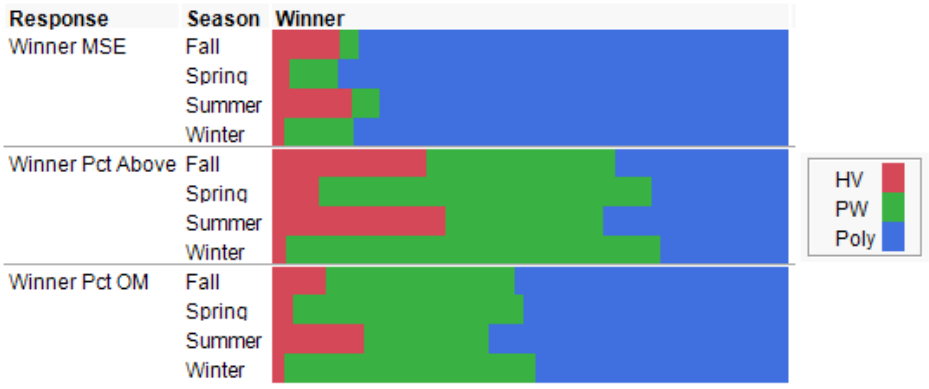

Figure 39. Model performance by season

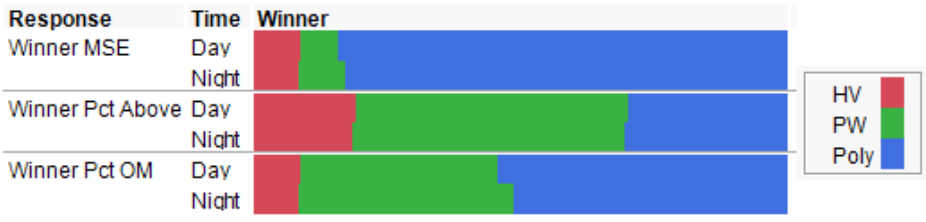

Figure 40. Model performance by time

The results are mostly in agreement with those found by the ANOVA. The H-V model exhibits the greatest change across zones and seasons. Invariance to time of day is emphasized by these charts.

V. Conclusion

5.1 Key Findings

Several important discoveries have emerged. Perhaps most significant is that tropopause heights are bimodal, with modes at approximately 10 and 17 km. Because a key component of standard optical turbulence models is the inflection at the tropopase, a single standard model does not effectively capture C_n^2 behavior.

The distinct drop-off in tropopause height at approximately 30 °N and 30 °S has been validated independently of this research. This gives reason for the use of different standard models in the polar and tropic regions.

The Hufnagel-Valley 5/7 model does a poor job of characterizing maritime C_n^2. It under-predicts the majority of values, and its tropopause inflection is uncharacteristic of the tropic region. Of the alternative models proposed, 9th order polynomial models perform the best overall. These models characterize C_n^2 in $\log_{10}$ space, unlike the H-V model which characterizes true values and maps to $\log_{10}$ space. The polynomial models also feature smaller fluctuations that deviate from theoretical behavior of turbulence. The proposed piecewise model is the most dynamic in nature, due to variable surface and tropopause values. However given the variable input parameters, its performance is somewhat underwhelming. This is in part the result of the criteria chosen for parameter selection.

5.2 Discussion and Future Research

This research provides a first attempt at proper characterization of maritime optical turbulence. Opportunities for extension are ample, as many avenues were unexplored.

Proper characterization of turbulence in the tropopause region is essential to model

building. Outside the tropic belt the observed data reveal a relationship between latitude and tropopause height, however extensive data collection is necessary to properly quantify the relationship. Magnitude of turbulence at the tropopause is also highly variable, however no significant relationship is apparent from the data. Inability to properly characterize these values has been manifested in the sub-optimal performance of the model. The effects of factors such as season and time of day on turbulence behavior (particularly in the tropopause) should continue to be studied to provide a more predictive model.

Additionally, an improvement on the method for determining tropopause height will aid in its characterization. The method used is effective, however extraneous variance is introduced for the instances where the inflection is misspecified.

To make the models (in particular the piecewise model) operationally useful, low-altitude turbulence characterization can be improved by calculating surface values in real time. Frederickson et al [15] showed that turbulence can be estimated with bulk methods using measured atmospheric conditions and sea temperature. Estimations are accurate when air temperature is lower than sea temperature (unstable conditions), but poor if the opposite is true (stable conditions). If unstable condtions are observed, measured surface values should be used as inputs to the piecewise model. Otherwise, observed bulk method values should be compared to polynomial model values to determine which are more appropriate. The Navy Surface Layer Optical Turbulence Model (NSLOT) is a maritime bulk method model that can be employed for this purpose. Implementing this change, piecewise model will likely outperform the polynomial model in the low-altitude region.

Turbulence in this study is calculated exclusively using AIRS-derived temperatures and NOMADS winds, however C_n^2 values found by AIRS temperatures and derived winds may be comparably useful. The level of agreement between AIRS and

AIRS/NOMADS turbulence is an open area of research. Meier (2010) found that AIRS winds are operationally sufficient; a similar study for AIRS-derived wind C_n^2 is yet to be completed.

Model building was completely empirical, relying only on observed measurements. Ideally, a theoretical approach aided with observations will result in arrival at a desired solution. For example, the relationship between wind speed at mid-altitude and optical turbulence is a theoretically-based characteristic of the H-V model that was not incorporated into the proposed models.

Any number of metrics can be used to compare models. MSE is commonly used in modeling, whereas the other metrics were created for the context of the analysis performed. Because the goal of standard models is not traditional response prediction, an effort should be made to create metrics that convey and allow for stratification of model performance.

Finally, because extensive data collection and management are required, an effort should be made to store and access data methodically and efficiently. Computation times can be reduced by orders of magnitude by saving files in a format that can be read and loaded quickly by the analysis software used.

Bibliography

1. A. Tunick, N. Tikhonov, M. Vorontsov, and G. Carhart, "Characterization of optical turbulence (C_n^2) data measured at the ARL A_LOT facility," 2005.

2. R. E. Hufnagel, "Propagation through atmospheric turbulence," *The Infrared Handbook*, vol. 2, pp. 6.1–6.56, 1993.

3. A. D. Tunick, "The refractive index structure parameter/atmospheric optical turbulence model: (C_n^2)," 1998.

4. L. E. Gravley, "Comparison of climatological optical turbulence profiles to standard, statistical and numerical models using HELEEOS," 2006.

5. R. R. Beland, "Propagation through atmospheric optical turbulence," *Atmospheric Propagation of Radiation*, vol. 2, pp. 157–232, 1993.

6. C. L. Parkinson, "Aqua: An earth-observing satellite mission to examine water and other climate variables," *Geoscience and Remote Sensing, IEEE Transactions on*, vol. 41, no. 2, pp. 173–183, 2003.

7. D. C. Meier, "Application of satellite-derived wind profiles to joint precision airdrop system (JPADS) operations," Master's thesis, Air Force Institute of Technology, 2010.

8. E. J. Fetzer, B. H. Lambrigtsen, A. Eldering, H. H. Aumann, and M. T. Chahine, "Biases in total precipitable water vapor climatologies from atmospheric infrared sounder and advanced microwave scanning radiometer," *Journal of Geophysical Research: Atmospheres (1984–2012)*, vol. 111, no. D9, 2006.

9. J. Susskind, C. Barnet, J. Blaisdell, L. Iredell, F. Keita, L. Kouvaris, G. Molnar, and M. Chahine, "Accuracy of geophysical parameters derived from atmospheric infrared sounder/advanced microwave sounding unit as a function of fractional cloud cover," *Journal of Geophysical Research: Atmospheres (1984–2012)*, vol. 111, no. D9, 2006.

10. G. K. Rutledge, J. Alpert, and W. Ebisuzaki, "NOMADS: A climate and weather model archive at the national oceanic and atmospheric administration," *Bulletin of the American Meteorological Society*, vol. 87, no. 3, pp. 327–341, 2006.

11. D. C. Meier and S. T. Fiorino, "Correlated satellite-derived turbulence, clouds & aerosol data," in *Propagation through and Characterization of Distributed Volume Turbulence (pcDVT), Imaging and Applied Optics Conference*, (Seattle, WA), 2014.

12. D. C. Montgomery, E. A. Peck, and G. G. Vining, *Introduction to Linear Regression Analysis*. New Jersey: John Wiley & Sons, 5th ed., 2012.

13. "Piecewise cubic hermite interpolating polynomial (PCHIP)." Last accessed on 24 Feb, 2015 at `http://www.mathworks.com/help/matlab/ref/pchip.html`.

14. T. Birner, S. M. Davis, and D. J. Seidel, "The changing width of earths tropical belt," *Physics Today*, vol. 67, no. 12, 2014.

15. P. A. Frederickson, K. L. Davidson, C. R. Zeisse, and C. S. Bendall, "Estimating the refractive index structure parameter (C_n^2) over the ocean using bulk methods," *Journal of applied meteorology*, vol. 39, no. 10, pp. 1770–1783, 2000.

REPORT DOCUMENTATION PAGE

Form Approved
OMB No. 0704–0188

1. REPORT DATE *(DD–MM–YYYY)*	2. REPORT TYPE	3. DATES COVERED *(From — To)*
26–03–2015	Master's Thesis	Sept 2013 — Mar 2015

4. TITLE AND SUBTITLE

DEVELOPMENT OF A STANDARD MARITIME C_N^2 PROFILE USING SATELLITE MEASUREMENTS

5a. CONTRACT NUMBER

5b. GRANT NUMBER

5c. PROGRAM ELEMENT NUMBER

6. AUTHOR(S)

Anderson, Gregory M, Second Lieutenant, USAF

5d. PROJECT NUMBER

5e. TASK NUMBER

5f. WORK UNIT NUMBER

7. PERFORMING ORGANIZATION NAME(S) AND ADDRESS(ES)

Air Force Institute of Technology
Graduate School of Engineering and Management (AFIT/EN)
2950 Hobson Way
WPAFB OH 45433-7765

8. PERFORMING ORGANIZATION REPORT NUMBER

AFIT-ENP-MS-15-M-141

9. SPONSORING / MONITORING AGENCY NAME(S) AND ADDRESS(ES)

Intentionally left blank

10. SPONSOR/MONITOR'S ACRONYM(S)

11. SPONSOR/MONITOR'S REPORT NUMBER(S)

12. DISTRIBUTION / AVAILABILITY STATEMENT

Distribution Statement A. Approved for Public Release; Distribution Unlimited.

13. SUPPLEMENTARY NOTES

14. ABSTRACT

The Hufnagel-Valley (H-V) 5/7 model was developed to characterize optical turbulence (C_n^2) as it varies with height over land. While the H-V 5/7 model is not meant to predict precise values, observations will likely be in a range close to the models prediction. H-V 5/7 is not suitable for modeling turbulence over the ocean, and to date no ocean profiles have been developed. The primary objective of this research is to develop a H-V-like standard maritime model of optical turbulence, and test its ability to accurately characterize C_n^2 over a broad spatial and temporal range. Maritime temperature climatology data are obtained from the Atmospheric Infrared Sounder (AIRS) aboard NASA's Aqua satellite. Three standard models are proposed as alternatives to the H-V model. Results show that maritime profiles generally do not exhibit the surface spike in turbulence seen in H-V 5/7. Additionally, a strong latitudinal variation in the height of the C_n^2 inflection associated with the tropopause is observed, motivating the need for separate models for polar and tropic regions.

15. SUBJECT TERMS

Optical turbulence, Hufnagel-Valley, Standard turbulence profile (H-V), H-V 5/7, High-energy laser (HEL), Model fitting, Regression

16. SECURITY CLASSIFICATION OF:			17. LIMITATION OF ABSTRACT	18. NUMBER OF PAGES	19a. NAME OF RESPONSIBLE PERSON
a. REPORT	b. ABSTRACT	c. THIS PAGE			Steven T. Fiorino, AFIT/ENP
U	U	U	U	60	19b. TELEPHONE NUMBER *(include area code)* (937) 255-3636, x4506; steven.fiorino@afit.edu